BIOCHEMISTRY
including biophysical chemistry & molecular biology

Article

pubs.acs.org/biochemistry

Structure of the USP15 N-Terminal Domains: A β-Hairpin Mediates Close Association between the DUSP and UBL Domains

Stephen Harper,[†] Tabot M. D. Besong,[‡] Jonas Emsley,[†] David J. Scott,[‡] and Ingrid Dreveny*[,†]

[†]Centre for Biomolecular Sciences, University of Nottingham, University Park Campus, Nottingham, NG7 2RD, United Kingdom
[‡]School of Biosciences, University of Nottingham, Sutton Bonington Campus, Sutton Bonington, LE12 5RD, United Kingdom

Supporting Information

ABSTRACT: Ubiquitin specific protease 15 (USP15) functions in COP9 signalosome mediated regulation of protein degradation and cellular signaling through catalyzing the ubiquitin deconjugation reaction of a discrete number of substrates. It influences the stability of adenomatous polyposis coli, IκBα, caspase-3, and the human papillomavirus type 16 E6. USP15 forms a subfamily with USP4 and USP11 related through a shared presence of N-terminal "domain present in ubiquitin specific proteases" (DUSP) and "ubiquitin-like" (UBL) domains (DU subfamily). Here we report the 1.5 Å resolution crystal structure of the human USP15 N-terminal domains revealing a 80 Å elongated arrangement with the DU domains aligned in tandem. This architecture is generated through formation of a defined interface that is dominated by an intervening β-hairpin structure (DU finger) that engages in an intricate hydrogen-bonding network between the domains. The UBL domain is closely related to ubiquitin among β-grasp folds but is characterized by the presence of longer loop regions and different surface characteristics, indicating that this domain is unlikely to act as ubiquitin mimic. Comparison with the related murine USP4 DUSP-UBL crystal structure reveals that the main DU interdomain contacts are conserved. Analytical ultracentrifugation, small-angle X-ray scattering, and gel filtration experiments revealed that USP15 DU is monomeric in solution. Our data provide a framework to advance study of the structure and function of the DU subfamily.

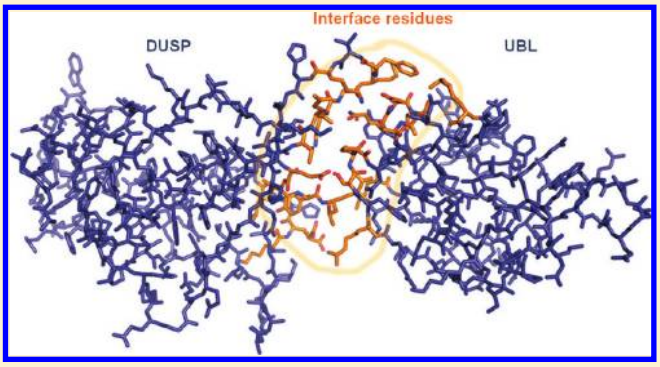

Ubiquitin specific proteases (USPs) have emerged as key regulators of ubiquitin mediated protein degradation and signaling,[1,2] thereby influencing major cellular events such as cell cycle progression, transcriptional regulation, and DNA damage repair. Dysfunction and mutation in USPs are linked to a number of diseases including neurodegenerative disease and cancer.[3,4] USPs share a papain-like proteolytic core domain of typically 30% sequence identity that harbors different insertions.[5,6] In addition, most USPs harbor functional domains at the N and/or C-terminus, such as typical ubiquitin binding domains and a range of other domains that probably mediate protein and ligand interactions to contribute to substrate specificity or cellular localization.[7,8] However, our functional and structural understanding of these variable domains is limited at present. USP15 is characterized by an N-terminal "domain present in ubiquitin specific proteases" (DUSP) followed by a predicted "ubiquitin-like domain" (UBL) upstream of the protease domain; neither of these domains have yet been assigned a function. USP15 associates with the COP9 signalosome[9,10] and thereby stabilizes tumor suppressor protein adenomatous polyposis coli,[11] regulates the RING-box protein Rbx1,[9] and influences the stability and activity of caspase-3 during Paclitaxel-induced apoptosis.[12] USP15 has also been implicated in the correct processing of polyubiquitinated substrates bound to p97.[13] Moreover, USP15 plays a role in the downregulation of NF-κB pathway through deubiquitinating NF-κB inhibitor IκBα[14,15] and also regulates human papillomavirus type 16 E6 oncoprotein stability.[16]

Among USPs, USP15 is most closely related to USP4[17,18] which has recently been implicated in mRNA splicing[19] and more distantly to USP11 which has been linked to DNA damage repair pathways.[20] The subfamily of USP15, USP4, and USP11 shares the same overall domain organization characterized by the presence of N-terminal DUSP and UBL domains (DU subfamily). There are currently no interaction partners known for the USP15 DU domains, but recently it has been shown that a region of USP4 including the N-terminal domains is responsible for the interactions with Sart3[19] which is involved in mRNA splicing.

The DUSP domain has been predicted in seven different USPs and occurs in duplicate or in combination with a UBL domain.[21] The NMR solution structure of the human USP15 DUSP domain has been determined previously, revealing a three-helix bundle supporting a triple-stranded antiparallel β-

Received: May 10, 2011
Revised: August 17, 2011
Published: August 17, 2011

Table 1. Data Collection and Refinement Statistics

data collection		refinement	
space group	$P3_121$	R_{factor}[c] (%)	15.6
cell parameters (Å)	$a = b = 97.60$, $c = 69.40$	R_{free}[d] (%)	17.8
wavelength (Å)	0.9763	no. of residues	222
D_{min} (Å)	1.48	ligand	1 sulfate
completeness (%)[a]	99.7 (97.9)	waters	363
total reflections	671 008	⟨B-factors⟩ (Å^2)	
unique reflections	63 890	protein	19.5
multiplicity[a]	10.5 (9.1)	waters	33
$\langle I/\sigma I\rangle$[a]	22.5 (6.7)	Ramachandran plot[e]	
Wilson plot B-factor (Å^2)	17.3	favored regions (%)	97.73
R_{merge}[b] (%)[a]	6.4 (29.2)	allowed regions (%)	2.27

[a]Values in parentheses are from the highest resolution shell (1.48−1.56 Å). [b]$R_{merge} = (\sum|I - \langle I\rangle|)/(\sum\langle I\rangle)$. [c]Crystallographic R factor = $(\sum|F_{obs} - F_{calc}|)/(\sum F_{obs})$ calculated with 90.1% of the data. [d]R_{free} is the R factor based on 9.9% of the data excluded from refinement. [e]Ramachandran plot statistics were calculated using MOLPROBITY.[33]

sheet.[21] The predicted presence of two UBL domains in USP15, USP4, and USP11 is intriguing.[5] UBL domains in multiple domain proteins often act as protein interaction modules.[22,23] In USP14, for example, the UBL domain has been shown to interact with the proteasome.[24] As USPs recognize ubiquitinated and ubiquitin substrates, an autoinhibitory role for these UBL domains as ubiquitin mimic in USPs has been suggested[5] and recently confirmed for the UBL domain located in an insertion of the protease domain of USP4.[25] In an effort to elucidate the arrangement and function of the N-terminal domains in USP15, we determined the crystal structure of the N-terminal domains directly upstream of the catalytic core domain. Our data reveal a unique tandem arrangement of the DUSP and UBL domains which is conserved in USP4 but not in USP11.

MATERIALS AND METHODS

Cloning, Expression, and Purification. Human USP15 corresponding to residues 1−222 (USP15 DU) was amplified from I.M.A.G.E. clone 40118994 and cloned into expression vector pET26b using NdeI and XhoI restrictions sites. The sequence verified plasmid was transformed into BL21 (DE3) codon plus cells (Stratagene). Bacterial cultures were grown at 37 °C to an OD of 0.6, induced with 1 mM IPTG, and grown for a further 3 h before centrifugation. Bacterial pellets were resuspended in 50 mM Tris-Cl pH 8, 150 mM NaCl, 25 mM imidazole, lysed, centrifuged, and loaded onto a HiTrap chelating column (GE Healthcare) precharged with $NiSO_4$. Elution was carried out using a gradient to 100% 50 mM Tris-Cl, 150 mM NaCl, pH 8, and 500 mM imidazole. Appropriate fractions were pooled, concentrated, and subsequently loaded on a Superdex 75 16/60 column (GE Healthcare) pre-equilibrated with 50 mM Tris-Cl, pH 7.4, 150 mM NaCl. Peak fractions were pooled and concentrated in Vivaspin concentrators (Sartorius) to 8.7 mg/mL for crystallization. Human USP4 (residues 1−226), USP4 DU, was cloned into pET26b using NdeI and XhoI restrictions sites. USP4 DU was expressed and purified using the same protocols as for USP15 DU. Unless otherwise indicated, all proteins correspond to the human sequence.

Protein Crystallization and Data Collection. Recombinant USP15 (residues 1−222) at a concentration of 8.7 mg/mL was used for sitting drop vapor diffusion crystallization trials at 20 °C by mixing equal amounts of USP15 (1−222) with precipitant solutions. Triangular-shaped crystals grew within a day in conditions of 2 M $(NH_4)_2SO_4$, 100 mM Bis-Tris-Cl at pH 5.5. Prior to flash cooling in liquid nitrogen, crystals were briefly soaked in a solution of 2.4 M $(NH_4)_2SO_4$, 100 mM Bis-Tris-Cl pH 5.5, and 30% glycerol. A data set to 1.5 Å resolution was collected at beamline I04, Diamond Light Source UK. Data were processed using the program iMOSFLM and scaled using SCALA.[26] Cell parameters and data collection statistics are summarized in Table 1.

Structure Solution, Model Building, Refinement, and Structure Analysis. The structure was solved by molecular replacement using the USP15 DUSP domain (PDB code 1W6V[21]) and the USP4 UBL domain (PDB code 3JYU, SGC) as search models with the CCP4 program PHASER.[27] Crystals contained one molecule per asymmetric unit with a solvent content of 65%. Model building was carried out using COOT.[28] The structure was refined with PHENIX[29] against a maximum likelihood target using translation/liberation/screw (TLS) refinement with parameters from the TLSMD web server in the final stages.[30] The final model contained 222 residues and 363 water molecules. The structure contains a sulfate molecule from the crystallization mother liquor. The quality of the electron density in the loop region between Asp^{73} and Gln^{77} is poor, probably due to multiple conformations; the main visible conformation supported by the density was modeled. Following Arg^{222}, the Leu-Glu sequence in the structure is a cloning artifact and is in fact occupied by Gly-Pro in USP15. The first three histidines from the affinity tag are also visible in the electron density. Refinement statistics as computed by PHENIX are tabulated in Table 1. The quality of the model was assessed using PROCHECK[31] (Supporting Information, Figure S1) and tools incorporated in the PHENIX package.[29] Model coordinates and structure factor files were deposited under accession number 3T9L in the Protein Data Bank. Figures were generated by PyMOL v0.99 (DeLano Scientific). ClustalW in combination with ESPript was used for sequence alignments and secondary structure assignments.[32] Prior to the analysis of interdomain contacts in murine USP4 DU, the PDB file 3JYU (Bacik et al., the SGC) was renumbered and modified by MOLPROBITY[33] to introduce side chain flips.

Small-Angle X-ray Scattering. USP15 (1−222) was expressed and purified according to the protocol described above and concentrated to 4.9 mg/mL for small-angle X-ray scattering (SAXS) data collection at beamline X33 at the DORIS-III storage ring at DESY Germany. Data were recorded using three different concentrations, 4.9, 2.5, and 1.6 mg/mL,

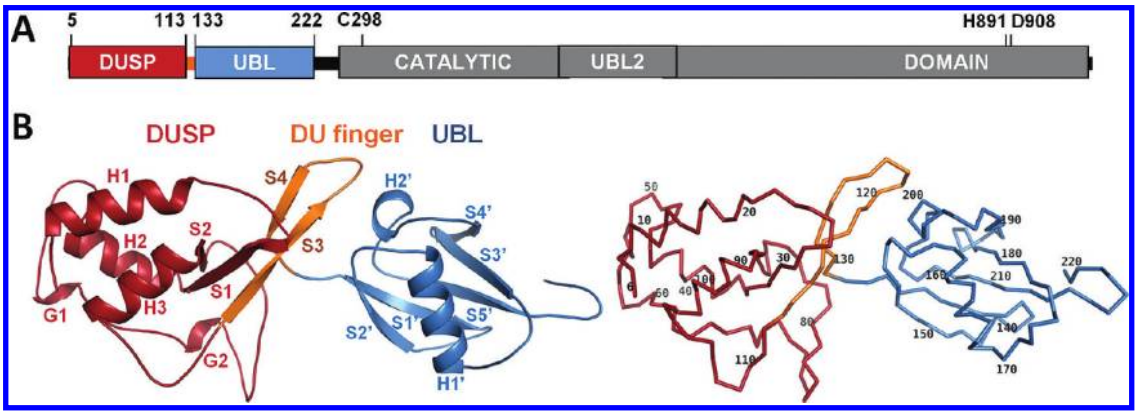

Figure 1. USP15 N-terminal domain structure. (A) Schematic representation of USP15 highlighting the overall domain organization and the location of catalytic residues (numbering refers to UniProt acc. code: Q9Y4E8). (B) USP15 DU domains in cartoon representation. The DUSP and UBL domains are depicted in red and blue, respectively. The DU finger β-hairpin structure at the interface of the two domains is highlighted in orange. Secondary structure elements are labeled according to the numbering scheme employed for the individual domains where H = α-helix, S = β-strand, and G = right-handed 3_{10} helix (left). Ribbon representation with every 10th residue labeled (right).

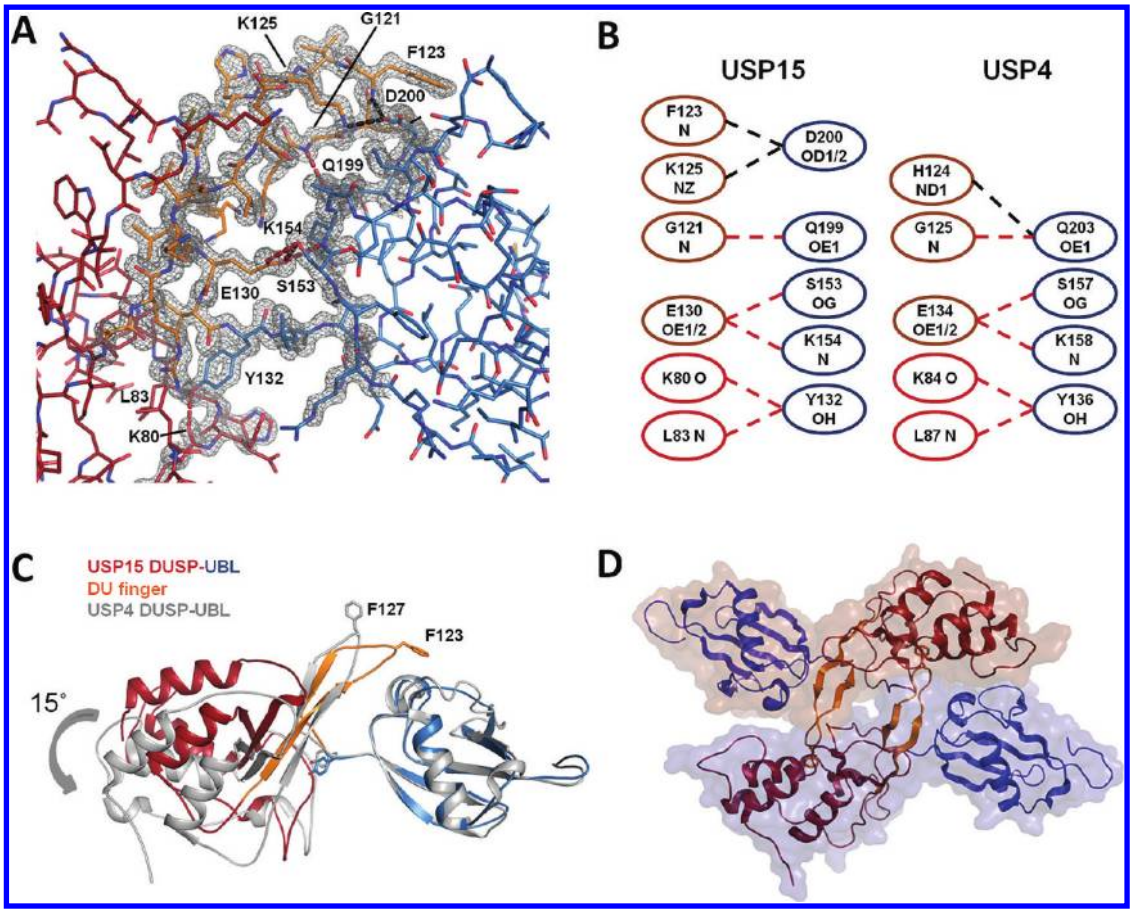

Figure 2. (A) Close-up stick representation of the DUSP UBL interface area with electron density map calculated using Fourier coefficients ($2F_{obs} - F_{calc}$), α_{calc} contoured at 1.7 sigma level. Key residues at the interface are labeled, and hydrogen-bonding interactions are shown as dashed lines. Color coding: red: present in USP15 and USP4 DU structures; black: present in USP15 DU structure. (B) Schematic representation of the hydrogen-bonding interactions at the USP15 and USP4 DU interfaces; color coding is the same as before. Note the absence of two hydrogen-bonding interactions at the tip of the USP4 DU finger. (C) Superposition of USP15 and USP4 (PDB code: 3JYU, SGC) DU structures based on the UBL domain. USP15 key residues Tyr^{132} and Phe^{123} at the interface are shown in stick representation. A slight difference in the DUSP domain orientation can be seen. (D) USP4 DU dimer as seen in the crystal structure (PDB code: 3JYU, SGC) shown in the same color scheme as USP15 DU. Note how Phe^{127} from one molecule inserts into a hydrophobic pocket in the DUSP domain of the other molecule. The solvent accessible surface area of the two molecules is shown in brown and blue, respectively.

intercepted by acquisition of buffer curves. The background was subtracted, and data were processed using the software package PRIMUS.[34] The final scattering curve used for calculation of *ab initio* models consisted of the highest concentration data merged with low Q sections from the lower concentration data. *Ab initio* models were calculated

dx.doi.org/10.1021/bi200726e | *Biochemistry* 2011, 50, 7995–8004

using the software DAMMIN and a final averaged molecular envelope was generated using the program DAMAVER. Subsequently, DAMFILT was used for filtering to obtain a representative dummy atom model.[34] The theoretical scattering curves for the USP15 DU crystal structure and a USP15 dimer model based on the USP4 crystal dimer (PDB code 3JYU, SGC) were generated and fitted to the experimental scattering curve using the program CRYSOL.[35] Domain fitting was carried out by superimposing the coordinate file with the dummy atom model using SUBCOMB.[34]

Analytical Ultracentrifugation. The USP15 N-terminal DU domains were expressed as described above, and solutions of 1, 0.5, and 0.25 mg/mL in 50 mM Tris-Cl, pH 7.4, 150 mM NaCl were prepared for ultracentrifugation studies. Sedimentation velocity experiments were carried out at 40 000 rpm using a Beckman XL-A analytical ultracentrifuge. Two channel sedimentation velocity cells were loaded into an An60Ti rotor; the set temperature was 20 °C. Partial specific volumes of the protein were calculated using SEDNTERP. Solution densities were measured using an Anton Paar DMA5000 density meter, and the solution viscosity measured using an Anton Paar microviscometer. Data were processed using ULTRASAN running on a Windows XP platform. Data were analyzed using the 2DSA and GA algorithms submitted to the Texas Teragrid using the LIMS portal contained in the ULTRASCAN software.

Gel Filtration Analysis. Purified USP15 and USP4 DU domains were analyzed by size exclusion chromatography using a Superdex 75 16/60 (GE Healthcare) equilibrated with 50 mM Tris-Cl, pH 7.4, 150 mM NaCl, 1 mM DTT, 1% glycerol (v/v). Protein samples of 1 mL at 8 mg/mL were applied and chromatographed at a flow rate of 0.8 mL/min. The column was calibrated using molecular weight standards (GE Healthcare): aprotinin, 6.5 kDa, V_e = 91.4 mL; ribonuclease A, 13.7 kDa, V_e = 77.2 mL; carbonic anhydrase, 29 kDa, V_e = 65.9 mL; ovalbumin, 44 kDa, V_e = 57.7 mL; conalbumin, 75 kDa, V_e = 51.9 mL. Peak fractions were collected, analyzed by SDS-PAGE, and visualized by Coomassie blue staining.

RESULTS

USP15 DUSP-UBL (DU) Structure. We cloned a USP15 construct spanning residues 1−222 that encompasses the N-terminal domains (Figure 1A). Crystallization screens yielded a single crystal form using 2 M $(NH_4)_2SO_4$, 100 mM Bis-Tris-Cl at pH 5.5 as mother liquor. Crystals have the symmetry of space group $P3_121$ with cell parameters of $a = b = 97.6$ Å, $c = 69.4$ Å and contain one molecule per asymmetric unit. The structure was determined using molecular replacement and refined to an R_{factor}/R_{free} of 15.6/17.8% at 1.5 Å resolution. The overall structure is kidney-shaped, measuring about 80 Å in the longest dimension (Figure 1B). The N-terminal DUSP domain is comprised of a three-helix bundle followed by a typical β-grasp fold ubiquitin-like (UBL) domain. The DUSP and UBL domains interact via a small interface forming an elongated arrangement. The previously determined NMR structure of the isolated USP15 DUSP domain (residues 6−132)[21] superimposes well on the crystal structure with an rmsd of 1.3 Å over 111 aligned Cα positions. Local differences occur in the loop regions Gly^{46}-Pro^{62} (following H2, Figure 1B) and Leu^{71}-Ser^{78} (following the 3_{10} helix G2). At the C-terminal end of the DUSP domain our crystal structure shows that strands S3 (Ile^{113} to Gln^{120}) and S4 (His^{126}-Val^{129}) adopt a distinctive β-hairpin structure (highlighted in orange in Figure 1B) which we will refer to as the DU finger. The tip of the DU finger is hydrophobic, consisting of residues Met^{122}, Phe^{123}, and Val^{124}. The DU finger tip is pinned to the side of the UBL domain via two hydrogen-bonding interactions between Phe^{123} main chain N and Asp^{200} as well as the Lys^{125} side chain and Asp^{200}. The interface is characterized by an extensive side chain−side chain and side chain−main chain hydrogen-bonding network along the length of the hairpin as shown in Figure 2A,B. Additional contacts also occur between Glu^{130} and Leu^{133}, Gly^{121} and Gln^{199}, Gln^{120} and Lys^{154}, Glu^{81} and Tyr^{132}, and Val^{118} and Ala^{155}. Furthermore, four water molecules are engaged in bridging the DUSP and UBL domains via hydrogen-bonding interactions. Overall, the DU interface buries a surface area of 380 Å^2 and is predominantly hydrophilic in nature, whereby the UBL domain contributes a positive electrostatic potential surface with contributions from residues Arg^{151} and Lys^{154} that is counteracted by a negative electrostatic potential on the DUSP surface through the presence of Glu^{81} and Glu^{130}. In addition to the DU finger, the DUSP domain loop regions prior to S2 are engaged in interactions with the UBL domain, whereas the UBL domain interface residues cluster within a stretch of sequence located between S2′ and H1′ and on H2′ (Figure 1B).

DU Interface Is Conserved in USP4. The closest homologue of USP15 is USP4,[36] and they share 58% sequence identity overall with 66% identity spanning the DU domains. Compared to USP15, USP4 harbors an additional four residues close to the N-terminus, and the residue numbering is respectively offset. We superposed the USP15 DU structure with the 2.4 Å resolution murine USP4 DU structure (PDB code 3JYU; Bacik et al., the SGC, mUSP4 1−229 crystallized in 20% w/v PEG 4000, 10% isopropanol, 0.1 M Na-HEPES, 1 mM DTT with two molecules in the asymmetric unit). The individual domains of USP15 and USP4 are similar overall and superimpose with an rmsd of 1.8 Å (DUSP; 119 matching Cα positions; 64% sequence identity) and 1.2 Å (UBL; 88 matching Cα positions; 72% sequence identity), respectively. Upon superposition of the DU structures via the UBL domains, the DUSP domains are offset by ∼15° (Figure 2C). The interface is conserved overall as schematically indicated in Figure 2B. The DU finger is present in USP4, and this sequence conserved with the exception of residues Leu^{126} and His^{124} replacing Met^{122} and Gln^{120} in USP15. Met^{122} is peripheral to the interface, and Gln^{120} is not in contact with the UBL domain. Although the residues at the finger tip are conserved, surprisingly, structural differences arise here in USP4 with Phe^{127} (Phe^{123} in USP15) peeling away from the body of the UBL and the tip extending away from the UBL domain. The phenylalanines at the tip of the turn adopt unusual dihedral angles in both structures. Concomitant changes in the interface resulting from this peeling back are illustrated schematically in Figure 2B, showing a reduction in the number of interfacial interactions formed in USP4. USP15 lacks a hydrogen-bonding interaction between His^{124} and Gln^{203} that occurs in USP4.

Analysis of DU Surface Features and Packing Interactions. The USP15 DU structure contains one molecule per asymmetric unit. We analyzed the USP15 DU crystal contacts using the PISA server.[37] This revealed the presence of two dimeric arrangements in the crystal packing; however, both involve only a small interface surface area (425 and 350 Å^2) within the range of a typical crystal contact. Unlike USP15 DU, USP4 DU forms an antiparallel dimer in the

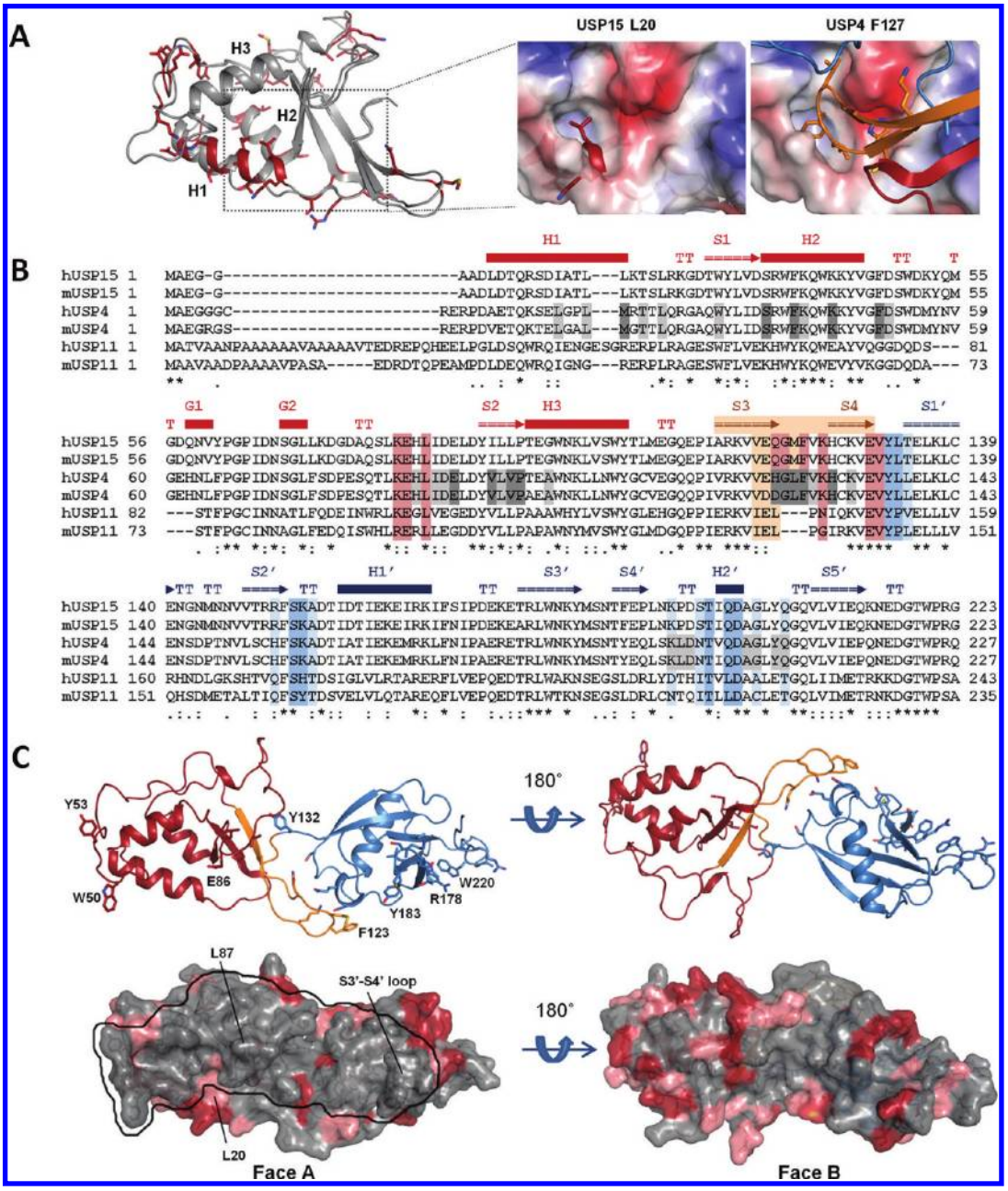

Figure 3. (A) Superposition of the hUSP15 and mUSP4 DUSP domain structures. USP15 residues that are not conserved in USP4 are depicted in red stick representation. Note the differences in helix 1. The boxed region is shown as a close-up on the right. USP4 electrostatic potential surface representation with USP15 Leu[20] shown that occludes the hydrophobic pocket present in USP4 (right). USP4 electrostatic surface area shown with USP4 Phe[127] from the second molecule in the crystallographic dimer occupying the hydrophobic pocket (far right). (B) Multiple sequence alignment of the N-terminal regions of hUSP15 (UniProt acc. code: Q9Y4E8); mUSP15 (UniProt acc. code: Q8R5H1); hUSP4 (UniProt acc. code: Q13107); mUSP4 (UniProt acc. code: P35123); hUSP11 (UniProt acc. code P51784), and mUSP11 (UniProt acc. code: Q99K46). USP15 secondary structure elements are shown above the sequences and color coded according to domains (red: DUSP; blue: UBL; shaded orange: DU finger). Residues shaded gray are located at the USP4 crystal dimer interface whereby dark gray denotes residues that are involved in direct contacts. Orange (DUSP) or light blue (UBL) shaded residues are located at the USP15 DUSP-UBL interface; red or dark blue shading denotes for direct contacts. (C) USP15 DU module structure shown in both cartoon (top) and surface (bottom) representation in the same orientation. Nonconserved residues between USP15 and USP4 sequences are depicted in red, similar residues depicted in salmon, and conserved residues depicted in gray. Note that one face of the molecule is significantly more conserved (face A, left and outlined) than the other (face B, right). Key residues referred to in the text are labeled.

asymmetric unit as shown in Figure 2D. A significant surface area of 1084 Å^2 is buried at the interface, which places it above 400−800 Å^2 generally observed for crystal contacts and the same order of magnitude as some obligate functional dimers.[38,39] There are no contributions from the UBL domain to the dimer interface apart from three residues forming a single surface patch, and the surfaces are not fully complementary in shape. In fact, the B chain UBL domain in the crystal is further removed and does not make any direct contacts with the DUSP domain of the A chain, resulting in a nonisologous dimer. In total, 10 residues from the A chain make direct contact with 13 residues from the B chain, and six residues are engaged in four

dx.doi.org/10.1021/bi200726e | *Biochemistry* 2011, 50, 7995−8004

hydrogen-bonding interactions according to DIMPLOT that uses HBPLUS.[40] A distinctive feature of the USP4 dimer interface is that the tip of the DU finger inserts into the hydrophobic pocket of the second DUSP domain lined by residues Met[24], Phe[42], Phe[51], Val[96], and Val[94] with the Phe[127] side chain fully buried and flanking Val[128] and Leu[126] side chains becoming partially buried. Figure 3A illustrates how USP15 Leu[20] from the N-terminal helix H1 has closed in to fill the pocket (right panel), whereas in USP4 H1 is shorter by three residues and slightly moved outward for the DU finger to insert (far right panel). Leu[20] is absolutely conserved in USP15 orthologues but replaced by methionine in most USP4 sequences.

Most residues contributing to the DUSP pocket region are conserved between USP15 and USP4. This includes the adjacent acidic residues Asp[85] and Glu[86] which line the rim of the pocket and are part of a β-turn that also contains the two exposed hydrophobic residues Ile[84] and Leu[87] (Figure 3). The exception is the N-terminal helix H1, which is the least conserved region between USP15 and USP4 DU domains (Figure 3B). Gly[21], the terminal residue of the shorter helix H1, is absolutely conserved among USP4 sequences but not present in USP15. Further analysis of the surface properties of USP15 DU in comparison with USP4 revealed that most absolutely conserved residues cluster on one face which contains the DUSP pocket (arbitrarily defined as face A and outlined in Figure 3C), whereas more variation is observed on the opposite face (face B in Figure 3C). The following noteworthy surface features locate to face A: (i) the USP15 loop region Phe[47]-Met[55] following H2 in the DUSP domain that adopts different conformations and contains Trp[50] and Tyr[53] (Figure 3C), residues that often occur at protein interfaces and rarely on the surface.[41] With the exception of Lys[52] that is replaced by Met[56] in USP4, this loop region is conserved across mammalian USP15 and USP4 sequences; (ii) the two exposed hydrophobic residues Ile[84] and Leu[87]; (iii) the UBL S3′−S4′ loop that is well ordered in USP15 due to crystal contacts but adopts different conformations with high B-factors in USP4; and (iv) Trp[220] from the C-terminal Asp-Gly-Thr-Trp-Pro motif that engages in a π-stacking interaction with the side chain of Arg[178] part of the Arg-Leu-Trp motif on strand S3′. Interestingly, these two motifs are not only strictly conserved between USP15 and USP4 but also in the more distantly related USP11 (Figure 3B).

Analysis of DU in Solution Using AUC and SAXS. To investigate the solution behavior of USP15 DU, we employed analytical ultracentrifugation (AUC) and small-angle X-ray scattering (SAXS) techniques. The sedimentation velocity experiments revealed a single species in solution (Figure 4A) with a hydrodynamic shape compatible with the crystal structure: the calculated sedimentation coefficient of 2.2 S is close to the experimental value of 2.4 S. An average molecular weight of 30 kDa was calculated, which agrees well with the theoretical molecular mass of 26.8 kDa.

SAXS experiments of USP15 DU revealed a molecular weight of 26 kDa (calculated from the forward scattering vector) consistent with a monomeric species. Buffer subtracted scattering curves and corresponding Guinier plots for USP15 DU at three concentrations are shown in Supporting Information, Figure S2. The radius of gyration, calculated by the second moment of the distance distribution function, and the maximum dimension, D_{max}, were found to be 26.6 and 81 Å, respectively: both values are consistent with the crystal

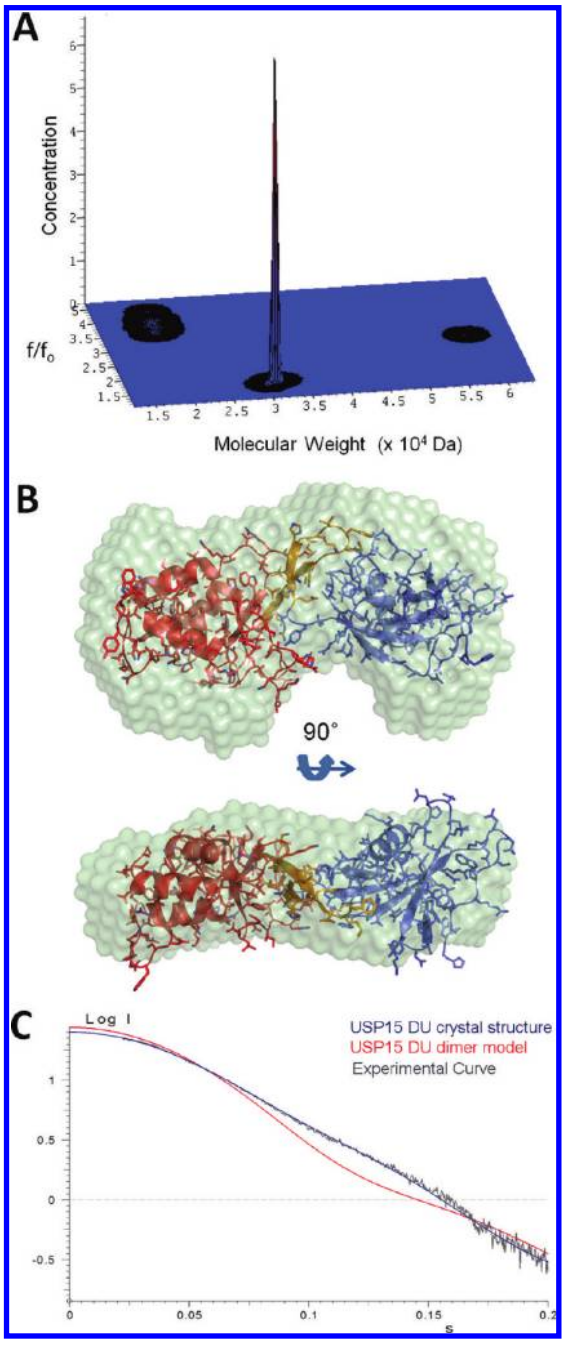

Figure 4. (A) Ultracentrifugation velocity sedimentation diagram of USP15 DUSP-UBL showing a single peak at a sedimentation coefficient of 2.4 S, corresponding to a monomer of USP15 with a molecular weight of 30 kDa. (B) USP15 DU crystal structure fitted into the SAXS *ab initio* molecular envelope using SUPCOMB. Two different orientations 90° from each other are shown. (C) Comparison of theoretical small-angle X-ray scattering curves derived from the USP15 DU crystal structure (blue) and a USP15 dimer model (red) computed using CRYSOL with the experimental scattering curve (gray). Note the near-perfect fit of the experimental curve with the monomeric USP15 DU crystal structure (chi^2 = 1.06) compared to the DU dimer model (chi^2 = 5.09).

structure ($R_{g,theor}$: 25.9 Å; longest dimension: 80 Å). We then reconstructed the molecular envelope of the protein using both small- and wide-angle scattering data. The results of ten independent runs of the reconstruction program DAMMIN[34] were used to construct a representative dummy atom model

dx.doi.org/10.1021/bi200726e | *Biochemistry* 2011, 50, 7995–8004

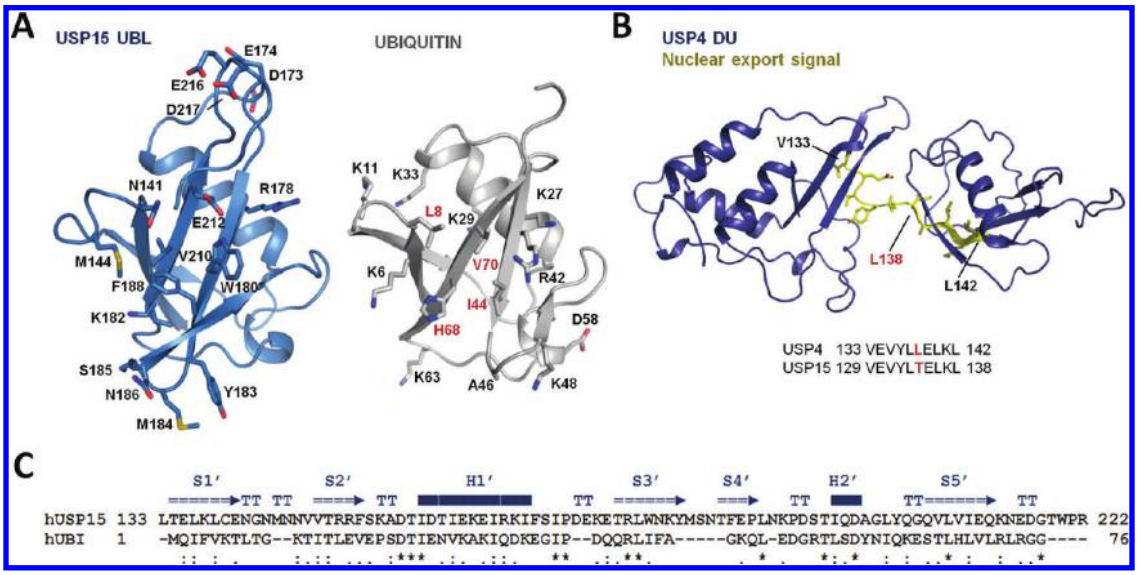

Figure 5. (A) USP15 UBL domain and ubiquitin shown in the same orientation with important residues labeled indicating the similarities and differences. Residues creating the hydrophobic surface patch in ubiquitin that most often engages in protein interactions are labeled red. (B) Location of the nuclear export signal in USP4, shown in yellow stick representation highlighting Leu[138] which is not conserved in USP15. (C) Structural alignment of human USP15 UBL and ubiquitin with secondary structure elements shown. Note the shorter loop regions in ubiquitin.

shown in Figure 4B. The molecular envelope agrees well with the shape of the crystal structure. The predicted scattering curve from the crystal structure matches the experimental one with a near ideal chi^2 value of 1.06 (Figure 4C). Slight differences can be attributed to the hydration shell and a degree of flexibility in loop regions and between the domains, such as seen between USP15 and USP4 DU. These results are in line with gel filtration, where pure USP15 DU monomer elutes at 68 mL corresponding to 27.5 kDa (Supporting Information, Figure S3).

We also investigated the behavior of USP4 DU in solution. Sedimentation velocity experiments on USP4 DU samples taken instantly post gel filtration revealed a single peak with a calculated sedimentation coefficient of 2.6 S, which correlates with an average molecular weight of 29.5 kDa (Supporting Information, Figure S4). Gel filtration of USP4 DU showed a main peak at 64.8 mL, corresponding to ~34 kDa (Supporting Information, Figure S3). These data are consistent with a monomeric species having a theoretical mass of 27.3 kDa. In contrast to USP15 DU, USP4 DU showed a tendency to self-associate/aggregate over time with higher order aggregates forming (unpublished observation).

Comparison of USP15 UBL with Other β-Grasp Folds.

In the USP15 DU structure, residues 133−218 adopt a ubiquitin-like fold. We performed structural comparisons of the UBL domain using DALI[42] which revealed that, apart from the USP4 UBL domain, the overall structure is most closely related to ubiquitin among UBL folds (*Z*-score of 11.0, PDB code 1TBE[43]). A *Z*-score of 11.4 with a lower sequence identity of 10% was obtained for tubulin folding cofactor B (PDB code 1T0Y[44]). The USP15 UBL domain can be superimposed onto ubiquitin (PDB code 1UBI[45]) with an rmsd of 2 Å and 18% sequence identity (75 matching Cα positions).

Overall, the USP15 UBL domain is characterized by longer loop regions compared to ubiquitin (Figure 5A). The loop connecting H1′ and S3′ and strand S3′ are significantly longer in USP15 UBL compared to ubiquitin. Similarly, the loop connecting strands 3 and 4 (S3′−S4′ loop), Ala[46]-Gly[47] in ubiquitin, is longer by three residues in USP15-UBL and consists of the sequence Tyr[183]-Met-Ser-Asn-Thr[187] (Figure 5A,C). Whereas ubiquitin is characterized by two surface regions of either predominantly positive electrostatic potential (front facing in Figure 5A), mediated through Arg[42], Arg[72], Lys[6], Lys[48], Arg[74] or negative electrostatic potential (back-facing in Figure 5A), through Asp[21] (Asp[156] in USP15), Glu[24] (Asp[159] in USP15), Asp[32] (Lys[167]), Glu[18] (Ser[153]), Glu[16] (Arg[151]), Asp[52] (Pro[194]), this charge distribution is not replicated in the UBL domain of USP15 as most residues are not conserved. A cluster of acidic residues creates a negative electrostatic potential in the area of the turn containing residues Glu[216] and Asp[217] and the turn containing Asp[173] and Glu[174] (between H1′ and S3′) in USP15. None of the ubiquitin lysine residues are conserved in the USP15 UBL domain, and there is no double glycine at equivalent positions in USP15 UBL. Residues creating the hydrophobic surface that acts as the main interaction site in ubiquitin,[46] namely around Ile[44], Val[70], Leu[8], and His[68], are not conserved in the USP15 UBL (Figure 5A,C). However, the corresponding region in USP15 is still hydrophobic in nature containing solvent exposed residues Trp[180] and Phe[188]. In addition, a leucine residue introduced by the cloning strategy interacts with this site. Ubiquitin Asp[58] engaged in the Rabex 5 interaction[47] is conserved in USP15 UBL (Asp[200]), but other residues in this region are not. Nor is ubiquitin His[68] conserved in USP15 which is involved in the interaction with the EAP45 GLUE domain.[48,49] Based on the sequence of the predicted second UBL domain within the catalytic protease domain of USP15, there are no obvious similarities to the N-terminal UBL domain (sequence identity of 11%). Similarly, other available USP UBL structures such as from USP7 (PDB code 2KVR, SGC, rmsd of 2.3 Å, and 9% sequence identity over 75 matching Cα positions) and murine USP14 (PDB code 1WGG, RSGI, rmsd of 1.9 Å, and 9% sequence identity over 64 matching Cα positions) do not share any obvious conserved surface features with USP15 UBL.

dx.doi.org/10.1021/bi200726e | *Biochemistry* 2011, 50, 7995−8004

DISCUSSION

There are at least 55 USPs in the human genome that have diverged to contain a plethora of ancillary domains proposed to mediate protein−protein interactions.[50] USPs are specific to certain substrates and ubiquitin chain linkages and often interact with ubiquitin ligases and other proteins as part of larger protein complexes.[8] Very little is known about the function and interaction partners of the N-terminal DUSP and UBL domains in USP15. We describe here the high resolution structure, surface characteristics, and solution behavior of the USP15 DU domains, utilizing X-ray crystallography, small-angle X-ray scattering, analytical ultracentrifugation, and gel filtration. We show that the two domains are arranged in tandem and that a distinct intervening β-hairpin structure mediates the interface between the DUSP and UBL domains. Interestingly, the β-hairpin is conserved in USP4 (PDB code 3JYU, SGC) where conformational changes may be important to expose the nuclear export signal (NES) that is located in this region (residues 133−141, Figure 5B).[17] Leu^{138} is replaced by Thr^{134} in USP15, and so far this sequence is not known to act as functional NES in USP15. We also noted that USP15 and USP4 share one face of the DU domains, arbitrarily termed face A that is distinctively more conserved than the other. This face is still largely exposed in the USP4 crystal dimer. It is tempting to speculate that this is of functional significance in the context of the full-length molecule or interaction with binding partners. Notably, this face contains the UBL S3′−S4′ loop which is absolutely conserved among mammalian USP15 and USP4 sequences (Figure 3B) but not other UBL domains found in USPs. This loop is often engaged in UBL protein−protein interactions.[23,24] The presence of surface hydrophobic residues such as USP15 Ile^{84} and Leu^{87}, Trp^{50} and Tyr^{53} also supports a functional role for face A.[41]

Overall, we observed three principal structural differences in a comparison of USP15 with USP4: (i) differences in orientation by about 15° between the DUSP and UBL domains; (ii) the DU finger loop packs closely onto the UBL domain in USP15 whereas it is extended away from the UBL in USP4, which results in a smaller interface; (iii) differences in the N-terminal helix H1 which is shortened in USP4. These differences may all be attributed to interactions with a second molecule in the crystal packing of the USP4 crystal structure which is not present in USP15. Although the DU finger is conserved, differences in the N-terminal helix impact on the DUSP domain pocket which may preclude such a dimer forming in USP15. The presence of a glycine residue that caps the N-terminal helix concomitant with the absence of a leucine residue in USP4 may aid in creating the deep hydrophobic pocket that can accept hydrophobic ligands/residues. Although the cleft in USP15 lacks this deep pocket, the hydrophobicity is conserved in this region. We anticipate that other DUSP domains will modulate the characteristics of this pocket through sequence variations in the N-terminal helix to create surface cavities that mediate binding to different ligands or the creation of self-association sites.

Our gel filtration, SAXS, and AUC experiments reveal that USP15 DU exists as a monomer in solution under physiological buffer conditions. We cannot rule out that there might be conditions under which H1 in the USP15 DUSP domain undergoes conformational changes to allow similar dimer formation as seen in the USP4 crystal structure, but as we observe both DU modules as predominantly monomeric in solution, the physiological relevance remains to be determined. In this context it is interesting to note that full length USP15 from *Rattus norvegicus* (98% sequence identity to human enzyme) has been reported to exist as monomer in solution,[51] whereas full-length cellular human USP4 has been shown to exist as monomer or higher molecular weight species.[52] This has mainly been attributed to USP4 associating with other proteins such as pRb but could also reflect transient dimerization. Alternatively, the crystal contacts observed in the murine USP4 DU structure may mimic a ligand. At this point there is no evidence for a functional role of the DUSP pocket or N-terminal UBL domain in the DU family, but the DUSP domain pocket is a potential site for protein−protein interactions.

Given the significant differences in surface characteristics between ubiquitin and the UBL domain, it is unlikely that the USP15 N-terminal UBL domain may act as ubiquitin mimic. Ubiquitin is generally recognized through the Ile^{44} face when interacting with USPs,[24,53,54] and based on our analysis, this surface in USP15 UBL, although hydrophobic, is very different in shape compared to ubiquitin. No obvious sequence and surface characteristics are shared between the structures of USP15, USP14, and USP7 UBL domains, the two other USP UBL structures that have been determined to date (SGC, RSGI). In the N-terminal USP14 UBL domain, which has been shown to interact with the proteasome,[24] the UBL S3′-S4′ loop is short like in ubiquitin, typically indicative of a better mimic of a β-grasp modifier,[23] whereas it is longer in the DU module of USP15 and USP4. These differences are in line with a proteomics study which shows that there are no common interaction partners known between USP14 and USP15.[55] Also, an interaction of USP15 with the proteasome has not been reported, indicating that these UBL domains may fulfill different functions.

There are significantly less structures of integral UBL domains showing interactions with adjacent domains compared to isolated UBL domain structures. Among these, the USP15 UBL domain interacts with the DUSP domain through a UBL surface area that is rarely used as recognition site,[56] which leaves the more typical sites available for potential interaction partners. The domain organization of an N-terminal DUSP followed by a UBL domain upstream of the protease domain is common to USP15, USP4, the more distantly related USP11 (32% sequence identity). Interestingly, based on sequence alignments, the DU finger β-hairpin in USP11 is shortened by three residues compared to USP15 and USP4 (Figure 3B), and not all residues engaged in interdomain contacts are conserved, which leads us to speculate that USP11 DU may adopt a different DU architecture.

A large-scale proteomics approach has identified proteins that interact with USPs and has shown that USP15 and USP4 have several interaction partners in common.[55] This is consistent with our findings that both share a common tandem DU architecture and some similarities in surface characteristics. These data will make a significant contribution to interpreting studies on ligand binding and the function of the DU domains in ubiquitin deconjugation and COP9 signalosome mediated processes.

ASSOCIATED CONTENT

Supporting Information

Supplementary figures provide information on the electron density of Ramachandran outliers according to PROCHECK[31]

(Figure S1), SAXS scattering curves used for computing *ab initio* models (Figure S2), the USP15 DU and USP4 DU protein samples used (Figure S3), and AUC data on USP4 DU (Figure S4). This material is available free of charge via the Internet at http://pubs.acs.org.

AUTHOR INFORMATION

Corresponding Author

*E-mail: ingrid.dreveny@nottingham.ac.uk. Tel: +44 1158468015. Fax: +44 1158468002.

Funding

This work was supported by the Biotechnology and Biological Sciences Research Council, Grant BB/H012656/1, the Royal Society, and the University of Nottingham. D.J.S. is grateful for a Beamtime award for access to DESY.

ACKNOWLEDGMENTS

We thank Wu Man Lung, Paulina Cygan, and Philippe Stivanin for assistance in the early stages of this work and the beamline scientists of I04, and Diamond Light Source UK, for their help during the synchrotron visit and for access to beamline I04.

ABBREVIATIONS

USP, ubiquitin specific protease; UBL, ubiquitin-like domain; DUSP, domain present in ubiquitin specific proteases; DU, DUSP-UBL; SAXS, small-angle X-ray scattering; AUC, analytical ultracentrifugation.

REFERENCES

(1) Kim, J. H., Park, K. C., Chung, S. S., Bang, O., and Chung, C. H. (2003) Deubiquitinating enzymes as cellular regulators. *J. Biochem. 134*, 9−18.

(2) Nijman, S. M., Luna-Vargas, M. P., Velds, A., Brummelkamp, T. R., Dirac, A. M., Sixma, T. K., and Bernards, R. (2005) A genomic and functional inventory of deubiquitinating enzymes. *Cell 123*, 773−786.

(3) Sacco, J. J., Coulson, J. M., Clague, M. J., and Urbe, S. (2010) Emerging roles of deubiquitinases in cancer-associated pathways. *IUBMB Life 62*, 140−157.

(4) Singhal, S., Taylor, M. C., and Baker, R. T. (2008) Deubiquitylating enzymes and disease. *BMC Biochem. 9* (Suppl. 1), S3.

(5) Zhu, X., Menard, R., and Sulea, T. (2007) High incidence of ubiquitin-like domains in human ubiquitin-specific proteases. *Proteins 69*, 1−7.

(6) Ye, Y., Scheel, H., Hofmann, K., and Komander, D. (2009) Dissection of USP catalytic domains reveals five common insertion points. *Mol. Biosyst. 5*, 1797−1808.

(7) Komander, D., Clague, M. J., and Urbe, S. (2009) Breaking the chains: structure and function of the deubiquitinases. *Nat. Rev. Mol. Cell Biol 10*, 550−563.

(8) Ventii, K. H., and Wilkinson, K. D. (2008) Protein partners of deubiquitinating enzymes. *Biochem. J. 414*, 161−175.

(9) Hetfeld, B. K., Helfrich, A., Kapelari, B., Scheel, H., Hofmann, K., Guterman, A., Glickman, M., Schade, R., Kloetzel, P. M., and Dubiel, W. (2005) The zinc finger of the CSN-associated deubiquitinating enzyme USP15 is essential to rescue the E3 ligase Rbx1. *Curr. Biol. 15*, 1217−1221.

(10) Zhou, C., Wee, S., Rhee, E., Naumann, M., Dubiel, W., and Wolf, D. A. (2003) Fission yeast COP9/signalosome suppresses cullin activity through recruitment of the deubiquitylating enzyme Ubp12p. *Mol. Cell 11*, 927−938.

(11) Huang, X., Langelotz, C., Hetfeld-Pechoc, B. K., Schwenk, W., and Dubiel, W. (2009) The COP9 signalosome mediates beta-catenin degradation by deneddylation and blocks adenomatous polyposis coli destruction via USP15. *J. Mol. Biol. 391*, 691−702.

(12) Xu, M., Takanashi, M., Oikawa, K., Tanaka, M., Nishi, H., Isaka, K., Kudo, M., and Kuroda, M. (2009) USP15 plays an essential role for caspase-3 activation during Paclitaxel-induced apoptosis. *Biochem. Biophys. Res. Commun. 388*, 366−371.

(13) Cayli, S., Klug, J., Chapiro, J., Frohlich, S., Krasteva, G., Orel, L., and Meinhardt, A. (2009) COP9 signalosome interacts ATP-dependently with p97/valosin-containing protein (VCP) and controls the ubiquitination status of proteins bound to p97/VCP. *J. Biol. Chem. 284*, 34944−34953.

(14) Schweitzer, K., Bozko, P. M., Dubiel, W., and Naumann, M. (2007) CSN controls NF-kappaB by deubiquitinylation of IkappaBalpha. *EMBO J. 26*, 1532−1541.

(15) Reyes-Turcu, F. E., Ventii, K. H., and Wilkinson, K. D. (2009) Regulation and cellular roles of ubiquitin-specific deubiquitinating enzymes. *Annu. Rev. Biochem. 78*, 363−397.

(16) Vos, R. M., Altreuter, J., White, E. A., and Howley, P. M. (2009) The ubiquitin-specific peptidase USP15 regulates human papillomavirus type 16 E6 protein stability. *J. Virol. 83*, 8885−8892.

(17) Soboleva, T. A., Jans, D. A., Johnson-Saliba, M., and Baker, R. T. (2005) Nuclear-cytoplasmic shuttling of the oncogenic mouse UNP/USP4 deubiquitylating enzyme. *J. Biol. Chem. 280*, 745−752.

(18) Baker, R. T., Wang, X. W., Woollatt, E., White, J. A., and Sutherland, G. R. (1999) Identification, functional characterization, and chromosomal localization of USP15, a novel human ubiquitin-specific protease related to the UNP oncoprotein, and a systematic nomenclature for human ubiquitin-specific proteases. *Genomics 59*, 264−274.

(19) Song, E. J., Werner, S. L., Neubauer, J., Stegmeier, F., Aspden, J., Rio, D., Harper, J. W., Elledge, S. J., Kirschner, M. W., and Rape, M. (2010) The Prp19 complex and the Usp4Sart3 deubiquitinating enzyme control reversible ubiquitination at the spliceosome. *Genes Dev. 24*, 1434−1447.

(20) Schoenfeld, A. R., Apgar, S., Dolios, G., Wang, R., and Aaronson, S. A. (2004) BRCA2 is ubiquitinated in vivo and interacts with USP11, a deubiquitinating enzyme that exhibits prosurvival function in the cellular response to DNA damage. *Mol. Cell. Biol. 24*, 7444−7455.

(21) de Jong, R. N., Ab, E., Diercks, T., Truffault, V., Daniels, M., Kaptein, R., and Folkers, G. E. (2006) Solution structure of the human ubiquitin-specific protease 15 DUSP domain. *J. Biol. Chem. 281*, 5026−5031.

(22) Hartmann-Petersen, R., and Gordon, C. (2004) Integral UBL domain proteins: a family of proteasome interacting proteins. *Semin. Cell. Dev. Biol. 15*, 247−259.

(23) Dreveny, I., Kondo, H., Uchiyama, K., Shaw, A., Zhang, X., and Freemont, P. S. (2004) Structural basis of the interaction between the AAA ATPase p97/VCP and its adaptor protein p47. *EMBO J. 23*, 1030−1039.

(24) Hu, M., Li, P., Song, L., Jeffrey, P. D., Chenova, T. A., Wilkinson, K. D., Cohen, R. E., and Shi, Y. (2005) Structure and mechanisms of the proteasome-associated deubiquitinating enzyme USP14. *EMBO J. 24*, 3747−3756.

(25) Luna-Vargas, M. P., Faesen, A. C., van Dijk, W. J., Rape, M., Fish, A., and Sixma, T. K. (2011) Ubiquitin-specific protease 4 is inhibited by its ubiquitin-like domain. *EMBO Rep. 12*, 365−372.

(26) Collaborative Computational Project, N.4 (1994) The CCP4 suite: programs for protein crystallography. *Acta Crystallogr., Sect. D: Biol. Crystallogr. 50*, 760−763.

(27) McCoy, A. J., Grosse-Kunstleve, R. W., Adams, P. D., Winn, M. D., Storoni, L. C., and Read, R. J. (2007) Phaser crystallographic software. *J. Appl. Crystallogr. 40*, 658−674.

(28) Emsley, P., Lohkamp, B., Scott, W. G., and Cowtan, K. (2010) Features and development of Coot. *Acta Crystallogr., Sect. D: Biol. Crystallogr. 66*, 486−501.

(29) Adams, P. D., Afonine, P. V., Bunkoczi, G., Chen, V. B., Davis, I. W., Echols, N., Headd, J. J., Hung, L. W., Kapral, G. J., Grosse-Kunstleve, R. W., McCoy, A. J., Moriarty, N. W., Oeffner, R., Read, R. J., Richardson, D. C., Richardson, J. S., Terwilliger, T. C., and Zwart, P. H. (2010) PHENIX: a comprehensive Python-based system for

macromolecular structure solution. *Acta Crystallogr., Sect. D: Biol. Crystallogr. 66*, 213−221.
(30) Painter, J., and Merritt, E. A. (2006) Optimal description of a protein structure in terms of multiple groups undergoing TLS motion. *Acta Crystallogr., Sect. D: Biol. Crystallogr. 62*, 439−450.
(31) Laskowski, R. A., MacArthur, M. W., Moss, D. S., and Thornton, J. M. (1993) PROCHECK: a program to check the stereochemical quality of protein structures. *J. Appl. Crystallogr.*, 283−291.
(32) Gouet, P., Robert, X., and Courcelle, E. (2003) ESPript/ENDscript: Extracting and rendering sequence and 3D information from atomic structures of proteins. *Nucleic Acids Res. 31*, 3320−3323.
(33) Chen, V. B., Arendall, W. B. III, Headd, J. J., Keedy, D. A., Immormino, R. M., Kapral, G. J., Murray, L. W., Richardson, J. S., and Richardson, D. C. (2010) MolProbity: all-atom structure validation for macromolecular crystallography. *Acta Crystallogr., Sect. D: Biol. Crystallogr. 66*, 12−21.
(34) Konarev, P. V., Petoukhov, M. V., Volkov, V. V., and Svergun, D. I. (2006) ATSAS 2.1, a program package for small-angle scattering data analysis. *J. Appl. Crystallogr. 39*, 277−286.
(35) Svergun, D. I., Barberato, C., and Koch, M. H. J. (1995) CRYSOL - a Program to Evaluate X-ray Solution Scattering of Biological Macromolecules from Atomic Coordinates. *J. Appl. Crystallogr.*, 768−773.
(36) Angelats, C., Wang, X. W., Jermiin, L. S., Copeland, N. G., Jenkins, N. A., and Baker, R. T. (2003) Isolation and characterization of the mouse ubiquitin-specific protease Usp15. *Mamm. Genome 14*, 31−46.
(37) Krissinel, E., and Henrick, K. (2007) Inference of macromolecular assemblies from crystalline state. *J. Mol. Biol. 372*, 774−797.
(38) Nooren, I. M., and Thornton, J. M. (2003) Diversity of protein-protein interactions. *EMBO J. 22*, 3486−3492.
(39) Janin, J., Rodier, F., Chakrabarti, P., and Bahadur, R. P. (2007) Macromolecular recognition in the Protein Data Bank. *Acta Crystallogr., Sect. D: Biol. Crystallogr. 63*, 1−8.
(40) Wallace, A. C., Laskowski, R. A., and Thornton, J. M. (1995) LIGPLOT: a program to generate schematic diagrams of protein-ligand interactions. *Protein Eng. 8*, 127−134.
(41) Chakrabarti, P., and Janin, J. (2002) Dissecting protein-protein recognition sites. *Proteins 47*, 334−343.
(42) Holm, L., and Sander, C. (1995) Dali: a network tool for protein structure comparison. *Trends Biochem. Sci. 20*, 478−480.
(43) Cook, W. J., Jeffrey, L. C., Kasperek, E., and Pickart, C. M. (1994) Structure of tetraubiquitin shows how multiubiquitin chains can be formed. *J. Mol. Biol. 236*, 601−609.
(44) Lytle, B. L., Peterson, F. C., Qiu, S. H., Luo, M., Zhao, Q., Markley, J. L., and Volkman, B. F. (2004) Solution structure of a ubiquitin-like domain from tubulin-binding cofactor B. *J. Biol. Chem. 279*, 46787−46793.
(45) Ramage, R., Green, J., Muir, T. W., Ogunjobi, O. M., Love, S., and Shaw, K. (1994) Synthetic, structural and biological studies of the ubiquitin system: the total chemical synthesis of ubiquitin. *Biochem. J. 299* (Pt. 1), 151−158.
(46) Sloper-Mould, K. E., Jemc, J. C., Pickart, C. M., and Hicke, L. (2001) Distinct functional surface regions on ubiquitin. *J. Biol. Chem. 276*, 30483−30489.
(47) Penengo, L., Mapelli, M., Murachelli, A. G., Confalonieri, S., Magri, L., Musacchio, A., Di Fiore, P. P., Polo, S., and Schneider, T. R. (2006) Crystal structure of the ubiquitin binding domains of rabex-5 reveals two modes of interaction with ubiquitin. *Cell 124*, 1183−1195.
(48) Alam, S. L., Langelier, C., Whitby, F. G., Koirala, S., Robinson, H., Hill, C. P., and Sundquist, W. I. (2006) Structural basis for ubiquitin recognition by the human ESCRT-II EAP45 GLUE domain. *Nat. Struct. Mol. Biol. 13*, 1029−1030.
(49) Hirano, S., Suzuki, N., Slagsvold, T., Kawasaki, M., Trambaiolo, D., Kato, R., Stenmark, H., and Wakatsuki, S. (2006) Structural basis of ubiquitin recognition by mammalian Eap45 GLUE domain. *Nat. Struct. Mol. Biol. 13*, 1031−1032.
(50) Quesada, V., Diaz-Perales, A., Gutierrez-Fernandez, A., Garabaya, C., Cal, S., and Lopez-Otin, C. (2004) Cloning and enzymatic analysis of 22 novel human ubiquitin-specific proteases. *Biochem. Biophys. Res. Commun. 314*, 54−62.
(51) Park, K. C., Choi, E. J., Min, S. W., Chung, S. S., Kim, H., Suzuki, T., Tanaka, K., and Chung, C. H. (2000) Tissue-specificity, functional characterization and subcellular localization of a rat ubiquitin-specific processing protease, UBP109, whose mRNA expression is developmentally regulated. *Biochem. J. 349*, 443−453.
(52) DeSalle, L. M., Latres, E., Lin, D., Graner, E., Montagnoli, A., Baker, R. T., Pagano, M., and Loda, M. (2001) The de-ubiquitinating enzyme Unp interacts with the retinoblastoma protein. *Oncogene 20*, 5538−5542.
(53) Hu, M., Li, P., Li, M., Li, W., Yao, T., Wu, J. W., Gu, W., Cohen, R. E., and Shi, Y. (2002) Crystal structure of a UBP-family deubiquitinating enzyme in isolation and in complex with ubiquitin aldehyde. *Cell 111*, 1041−1054.
(54) Renatus, M., Parrado, S. G., D'Arcy, A., Eidhoff, U., Gerhartz, B., Hassiepen, U., Pierrat, B., Riedl, R., Vinzenz, D., Worpenberg, S., and Kroemer, M. (2006) Structural basis of ubiquitin recognition by the deubiquitinating protease USP2. *Structure 14*, 1293−1302.
(55) Sowa, M. E., Bennett, E. J., Gygi, S. P., and Harper, J. W. (2009) Defining the human deubiquitinating enzyme interaction landscape. *Cell 138*, 389−403.
(56) Winget, J.M., and Mayor, T. (2010) The diversity of ubiquitin recognition: hot spots and varied specificity. *Mol. Cell 38*, 627−635.